Department of Physics and Astronomy
University of Heidelberg

Bachelor Thesis in Physics
submitted by **Rico Erhard**

born in Oberkirch

2015

Investigation of the Kapitza-Dirac effect in elliptically polarized fields

This Bachelor Thesis has been carried out by Rico Erhard at the
Max Planck Institute for Nuclear Physics (MPIK) in Heidelberg
under the supervision of
Honorarprof. Dr. Christoph H. Keitel

Abstract

The reflection of electrons from standing light waves is known as the Kapitza-Dirac effect. This thesis investigates the two-photon Kapitza-Dirac effect for electrons in the Bragg regime with elliptically polarized light fields. This means that the electrons can gather exactly two photon momenta in the standing light wave which is composed of two counterpropagating light waves of elliptical polarization. For this purpose, the time evolution of an electron is simulated by means of the Dirac equation in a one dimensional model. If the two light waves have equal helicity, the scattering process becomes suppressed for elliptical polarization and vanishes completely for circular polarization. If the two light waves have opposite helicity, the scattering is not suppressed and for sufficiently long interaction times spin effects arise that influence the scattering process. The spin expectation value of the electron oscillates and this oscillation is a superposition of two oscillations. These oscillations become fastest for circular polarization and vanish for linear polarization. It is shown that both cases can effectively be described by wave equations with time independent Hamiltonians. In the case of equal helicity the wave function obeys a Schrödinger equation while in the case of opposite helicity it obeys a Pauli equation with relativistic corrections.

Zusammenfassung

Die Streuung eines Elektronenstrahles an einer stehenden Lichtwelle wird als Kapitza-Dirac-Effekt bezeichnet. Diese Arbeit untersucht den zwei-Photonen-Kapitza-Dirac-Effekt in elliptisch polarisierten Feldern im Bragg-Regime. Dies bedeutet, dass ein Elektron bei Wechselwirkung mit der stehenden Lichtwelle, die aus zwei gegenläufigen elliptisch polarisierten Lichtwellen besteht, zwei Photonenimpulse erhalten kann. Zu diesem Zwecke wurde die Zeitentwicklung eines Elektrons in einem eindimensionalen Modell mithilfe der Dirac-Gleichung numerisch berechnet. Weisen die beiden Lichtwellen gleiche Helizität auf, kommt es zu einer Unterdrückung des Streuprozesses. Diese Unterdrückung wächst mit steigendem Grad der Elliptizität bis hin zur vollständigen Unterdrückung der Reflektionen bei zirkularer Polarisation. Haben die beiden Lichtwellen umgekehrte Helizität, findet diese Unterdrückung nicht statt. Dafür ist hier eine Spindynamik zu beobachten, die Einfluss auf den Streuprozess hat. Der Erwartungswert des Spins unterliegt einer Schwebung, die umso schneller wird je höher der Grad der Elliptizität wird. Bei linearer Polarisation gibt es diese Dynamik nicht. Beide Fälle lassen sich durch Wellengleichungen mit zeitunabhängigem Hamilton-Operator beschreiben. Im Falle gleicher Helizität lässt sich das Verhalten der Wellenfunktion durch eine Schrödinger-Gleichung beschreiben, im Falle umgekehrter Helizität durch eine Pauli-Gleichung mit relativistischen Korrekturen.

Contents

1 Introduction

1.1 What is the Kapitza-Dirac effect?

First predicted in 1933 by Pyotr Kapitza and Paul Dirac [1], the Kapitza-Dirac effect describes the diffraction of electrons on a standing light wave composed of two counterpropagating linearly polarized light waves of the same frequency. The principles governing the Kapitza-Dirac effect are not limited to electrons but include other particles as well.

While experimental evidence for light diffraction effects was found long before the 20^{th} century, first successful experimental confirmations of Kapitza's and Dirac's predictions were found not until 1986 [2, 3]. These experiments used sodium atoms. The first observation of the Kapitza-Dirac effect for electrons was made 1988 by Bucksbaum and others [4] in the diffractive regime whereas Batelaan and others [5] in 2001 could observe it in the Bragg regime. In the Bragg regime the particle has to impinge on the light wave at a certain angle (Bragg angle) in order to be scattered and the outgoing beam of scattered particles is detectable at a certain angle. In the diffractive regime the particle can be scattered into many different diffraction orders. See section 1.3 for more detailed information on those two regimes.

The long lapse between prediction and observation of the Kapitza-Dirac effect is mainly due to the very weak interaction between particle and light. Kapitza and Dirac estimated that the proportion of the deflected electrons would be only 10^{-14} for the intensity produced by a mercury arc lamp [1]. The development of the laser was therefore of utmost importance to render the effect observable in experiments, for its magnitude grows quadratically with the applied intensity.

1.2 Wave-particle duality

Wave-particle duality allows for two different interpretations of the Kapitza-Dirac effect that do not contradict each other. In wave theory the incoming electron beam can be described by de Broglie waves with an associated wavelength [6]. In this interpretation the standing light wave acts as an optical lattice for the incoming matter waves leading to interference phenomena. This grating is formed by nodes and antinodes of time dependent but periodic field strengths. In this sense, the role of light and matter is switched compared to phenomena where light diffracts on periodical structures of matter, for instance, crystals or gratings.

The other interpretation makes use of the particle aspect of both the electrons and the light. During interaction with the light an electron absorbs photons from one light wave

and subsequently emits photons stimulated by the other light wave. In doing so, the electrons gain integer multiples of twice the photon momentum along the propagation direction of the light beams.

1.3 Bragg regime and diffractive regime

Nowadays the term Kapitza-Dirac effect is used synonymously to designate phenomena that are more or less similar to the Kapitza-Dirac effect in Kapitza's and Dirac's original paper. Here it is useful to distinguish between two different regimes the Bragg regime and the diffractive regime. As already mentioned, the main difference between the two regimes is the number of possible diffraction orders that can be reached. While in Bragg scattering exactly one diffraction order can be reached similar to Bragg scattering on crystals, the diffractive regime allows for many diffraction orders similar to diffraction of light on an optical lattice.

The precise diffraction angles corresponding to precise incident and outgoing momenta in the Bragg regime are a direct consequence of conservation of energy and momentum. At first glance, it seems therefore as if energy-momentum conservation is violated in the diffractive regime. The uncertainty principle is the reason why this is not the case. There are quite a few uncertainty relations. One prominent example is the uncertainty relation $\Delta x \Delta p \geq \hbar/2$ relating position and momentum. Experimentally, one can switch between the two regimes by changing the light beam shape [3, 7]. In the diffractive regime a tightly focused light wave with a small waist leads to a small uncertainity in photon position. The inevitable big uncertainty in momentum enables conservation of energy and momentum for many final diffraction orders. In the Bragg regime this argumentation is reversed. A well collimated beam with large waist causes a big uncertainty in position which leads to a small uncertainty in momentum. Therefore the scattering process works only if a proper incident angle is chosen. Kapitza's and Dirac's paper [1] covers the so-called two-photon Kapitza-Dirac effect in the Bragg regime. Two photon means here that two photons are involved in the process. One photon that is absorbed by an electron plus one photon that is emitted subsequently by the same electron.

1.4 What is the purpose of this work?

For linear polarized light fields the Kapitza-Dirac effect is very well understood. The purpose of this work is to shed light on the implications that arise from circularly/elliptically polarized fields. In contrast to the two-photon Kapitza-Dirac effect for linearly polarized fields, spin effects may be of influence on the eletron diffraction as the angular momentum of light might couple to the electron spin.

2 Basics

2.1 Dirac equation

Note that all physical quantities in this document are given in atomic units unless otherwise mentioned. As the angular momentum $\hbar$ equals one in this unit system, it will be omitted completely. This section is intended to introduce the Dirac equation and the notation related to it. The Dirac equation is a relativistic wave equation which describes the quantum mechanics of spin $1/2$ particles. For a free particle it can be written as follows [8]

$$i\frac{\partial \psi}{\partial t} = \hat{\boldsymbol{H}}\psi, \tag{2.1}$$

with the free Dirac Hamiltonian $\hat{\boldsymbol{H}}$

$$\hat{\boldsymbol{H}} = c\boldsymbol{\alpha}\cdot\hat{\boldsymbol{p}} + mc^2\boldsymbol{\beta} \tag{2.2}$$

where $\hat{\boldsymbol{p}} = -i\nabla$ is the momentum operator and

$$\boldsymbol{\alpha}\cdot\hat{\boldsymbol{p}} = \sum_{k=1,2,3} \alpha_k p_k. \tag{2.3}$$

The requirement that the Dirac matrices $\boldsymbol{\alpha}$ and $\boldsymbol{\beta}$ are hermitian and that the Dirac Hamiltionian fulfills the energy-momentum relation $\hat{\boldsymbol{H}}^2 = c^2\boldsymbol{p}^2 + m^2c^4$ leads to

$$\boldsymbol{\alpha}_k\boldsymbol{\alpha}_j + \boldsymbol{\alpha}_j\boldsymbol{\alpha}_k = 2\delta_{k,j}\mathbf{1}, \tag{2.4}$$

$$\boldsymbol{\alpha}_k\boldsymbol{\beta} + \boldsymbol{\beta}\boldsymbol{\alpha}_k = \mathbf{0}, \tag{2.5}$$

$$\boldsymbol{\beta}^2 = 1, \quad k,j \in \{1,2,3\}, \tag{2.6}$$

in three dimensions. The standard representation

$$\boldsymbol{\alpha}_j = \begin{pmatrix} \mathbf{0}_2 & \sigma_j \\ \sigma_j & \mathbf{0}_2 \end{pmatrix}, \quad j \in \{1,2,3\}, \quad \boldsymbol{\beta} = \begin{pmatrix} \mathbf{1}_2 & \mathbf{0}_2 \\ \mathbf{0}_2 & -\mathbf{1}_2 \end{pmatrix}, \tag{2.7}$$

with the Pauli matrices

$$\sigma_1 = \begin{pmatrix} 0 & 1 \\ 1 & 0 \end{pmatrix}, \quad \sigma_2 = \begin{pmatrix} 0 & -i \\ i & 0 \end{pmatrix}, \quad \sigma_3 = \begin{pmatrix} 1 & 0 \\ 0 & -1 \end{pmatrix}, \tag{2.8}$$

fulfills the aforementioned relations. In this representation plane wave solutions for a free particle can be written [9] as

$$\psi^{+\uparrow,+\downarrow} = \sqrt{\frac{E+mc^2}{2E}} \begin{pmatrix} \chi^{\uparrow,\downarrow} \\ \frac{c\sigma p}{E+mc^2}\chi^{\uparrow,\downarrow} \end{pmatrix} e^{i(px-Et)}, \tag{2.9}$$

$$\psi^{-\uparrow,-\downarrow} = \sqrt{\frac{E+mc^2}{2E}} \begin{pmatrix} -\frac{c\sigma p}{E+mc^2}\chi^{\uparrow,\downarrow} \\ \chi^{\uparrow,\downarrow} \end{pmatrix} e^{i(px-Et)}, \tag{2.10}$$

$$\chi^{\uparrow} = \begin{pmatrix} 1 \\ 0 \end{pmatrix}, \quad \chi^{\downarrow} = \begin{pmatrix} 0 \\ 1 \end{pmatrix}, \quad E = \sqrt{m^2c^4 + p^2c^2}. \tag{2.11}$$

2.2 Minimal coupling and Foldy–Wouthuysen transformation

Classical electromagnetic fields are completely determined by the vector potential $\boldsymbol{A}$ and the scalar potential Φ via $\boldsymbol{E} = -\dot{\boldsymbol{A}} - \nabla\Phi$ and $\boldsymbol{B} = \nabla \times \boldsymbol{A}$. The substitutions

$$i\frac{\partial}{\partial t} \to i\frac{\partial}{\partial t} - q\,\Phi \tag{2.12a}$$

$$\boldsymbol{p} \to \hat{\boldsymbol{p}} - q\boldsymbol{A} \tag{2.12b}$$

in the Dirac equation allow for interactions with external fields

$$i\frac{\partial\psi}{\partial t} = \left(c\boldsymbol{\alpha}\cdot(\hat{\boldsymbol{p}} - q\boldsymbol{A}) + mc^2\boldsymbol{\beta} + q\Phi\right)\psi \tag{2.13}$$

where q is the charge of the particle. This procedure known as minimal coupling is common even outside quantum mechanics. However, a physical interpretation with respect to the electromagnetic fields $\boldsymbol{E}$ and $\boldsymbol{B}$ in this form proves rather difficult. In this regard, a Foldy–Wouthuysen transformation that is a non-relativistic expansion of equation (2.13) is more useful [10]:

$$\begin{aligned} i\frac{\partial\psi}{\partial t} = \Bigg[&\frac{1}{2m}(\hat{\boldsymbol{p}} - q\boldsymbol{A})^2 - \frac{q}{2m}\boldsymbol{B}\cdot\boldsymbol{\sigma} - \frac{q}{4m^2c^2}\boldsymbol{\sigma}\cdot(\boldsymbol{E}\times(\hat{\boldsymbol{p}} - q\boldsymbol{A})) \\ &+ mc^2 + q\Phi - \frac{q}{8m^2c^2}\nabla\boldsymbol{E} - \frac{1}{8m^3c^2}(\hat{\boldsymbol{p}} - q\boldsymbol{A})^4 \\ &+ \frac{q^2}{8m^3c^4}\left(\boldsymbol{E}^2 - c^2\boldsymbol{B}^2\right) + \frac{q}{8m^3c^2}\left\{(\hat{\boldsymbol{p}} - q\boldsymbol{A})^2, \boldsymbol{B}\cdot\boldsymbol{\sigma}\right\}\Bigg]\psi. \end{aligned} \tag{2.14}$$

Note that the spinor ψ is here a wave function of two components.

2.3 Angular momentum of light

As is widely known, light or electromagnetic waves in general carry energy and momentum. Less known is the angular momentum of light defined by

$$\boldsymbol{J} = \int_v \boldsymbol{r}\times(\boldsymbol{E}\times\boldsymbol{B})\,\mathrm{d}v \tag{2.15}$$

in a volume v with respect to the origin of the coordinate system with position vector $\boldsymbol{r}$. This angular momentum can be observed, for instance, by transferring it on a macroscopic object [11]. The total angular momentum can be split [12] into the sum

$$\boldsymbol{J} = \sum_i \int_v \boldsymbol{E}_i \boldsymbol{r} \times \boldsymbol{A}_i \,\mathrm{d}v + \int_v \boldsymbol{E} \times \boldsymbol{A} \,\mathrm{d}v - \int_s (\boldsymbol{r} \times \boldsymbol{A})(\boldsymbol{E} \times \boldsymbol{n}) \,\mathrm{d}s + \int_v (\boldsymbol{r} \times \boldsymbol{A}) \nabla \boldsymbol{E} \,\mathrm{d}v \tag{2.16}$$

where s is the surface of the volume v. The related surface normal vector is $\boldsymbol{n}$ and the vector potential $\boldsymbol{A}$ is given in Coulomb gauge which is also often referred to as transverse gauge and is defined by $\nabla \boldsymbol{A} = 0$. If $\boldsymbol{A}$ decreases to zero sufficiently fast and the volume v becomes larger and larger, the last two terms are negligible. In this case only the first two parts make up the angular momentum of light $\boldsymbol{J}$. While the first term bears the form of an orbital angular momentum, the second term has the form of an inherent momentum or spin, for it is independent of the point of reference. Therefore it is tempting to interpret the integrand of the spin angular momentum as a spin density. This is a controversial subject. An alternative approach [13] splits the total angular momentum (2.15) in a different manner. This yields the spin density $\frac{1}{2}(\boldsymbol{E} \times \boldsymbol{A} + \boldsymbol{B} \times \boldsymbol{C})$ in which the vector potential $\boldsymbol{C}$ is defined by $\boldsymbol{E} = -\nabla \times \boldsymbol{C}$ and $\boldsymbol{B} = -\dot{\boldsymbol{C}}$. Altough this differs from $\boldsymbol{E} \times \boldsymbol{A}$ the total spin angular momenta for the two different definitions coincide:

$$\int_v \frac{1}{2} \left(\boldsymbol{E} \times \boldsymbol{A} + \boldsymbol{B} \times \boldsymbol{C} \right) \mathrm{d}v = \int_v \boldsymbol{E} \times \boldsymbol{A} \,\mathrm{d}v. \tag{2.17}$$

For the electromagnetic fields used in this work even the densities coincide.

2.4 Resonance condition

The Kapitza-Dirac effect occurs in standing light waves that are composed of two counterpropagating light beams of the same frequency. The scattering of electrons in such a light wave as described in [1] for linear polarized light works as follows. An electron in the field absorbs a photon from one of the beams and subsequently emits it stimulated by the other beam. During this process an electron gains two photon momenta. The number of absorbed and emitted photons can be different from the case above but is not arbitrary. From energy and momentum conservation one can show [14] that an electron can only absorb photons from one light beam and emits photons into the other beam and that it has to fulfill the following resonance condition

$$p_{1,\mathrm{in}} = -\frac{n_\mathrm{a} + n_\mathrm{e}}{2} k \pm \frac{|n_\mathrm{a} - n_\mathrm{e}|}{2} \sqrt{k^2 + \frac{m'^2 c^2}{n_\mathrm{a} n_\mathrm{e}}} \tag{2.18}$$

where k is the wave number of the light and c its velocity, $p_{1,\mathrm{in}}$ is the initial momentum of the electron with respect to the optical axis which is the light propagation direction. The other two components of the electron momentum $p_{2,\mathrm{in}}$ and $p_{3,\mathrm{in}}$ are contained in the increased mass $m' = c^{-2}\sqrt{m^2c^4 + p_{2,\mathrm{in}}^2 c^2 + p_{3,\mathrm{in}}^2 c^2}$. The number of absorbed photons is n_a

while n_e is the number of emitted photons. In the two-photon Kapitza-Dirac effect, that is $n_a = n_e = 1$, equation (2.18) simplifies to

$$p_{1,\text{in}} = -k. \tag{2.19}$$

In this case, the initial momentum of the electron in light propagation direction has to be equivalent to one photon momentum. This corresponds to the fact that the electron has to impinge on the light wave at a certain angle ϑ

$$\cos\vartheta = \frac{k}{|\boldsymbol{p}_{\text{in}}|}, \tag{2.20}$$

or using de Broglie's wave-particle relation one obtains

$$\lambda_{e^-} = \lambda_{\text{Light}} \cos(\vartheta), \tag{2.21}$$

which is Bragg's law with a lattice spacing of $\lambda_{\text{Light}}/2$.

2.5 Setup

The physical setup consists of two counterpropagating elliptically polarized light waves forming a standing wave. Both light waves feature the same intensity, wave length and degree of ellipticity, but may differ in helicity. In the case of opposite helicity the fields (taken verbatim from [15]) are given by

$$\boldsymbol{E}_{1,2}^{\zeta\zeta} = \hat{E} \begin{pmatrix} 0 \\ \cos(kx \mp \omega t) \\ \cos(kx \mp \omega t \pm \eta) \end{pmatrix}, \tag{2.22a}$$

$$\boldsymbol{B}_{1,2}^{\zeta\zeta} = \frac{\hat{E}}{c} \begin{pmatrix} 0 \\ \mp\cos(kx \mp \omega t \pm \eta) \\ \pm\cos(kx \mp \omega t) \end{pmatrix}, \tag{2.22b}$$

in which $\hat{E}$ is a constant proportional to the amplitude, $k = 2\pi/\lambda$ denotes the wave number, x is the position along the optical axis, t is time and c the speed of light. Furthermore, $\omega = kc$ is the angular frequeny, $\eta \in (-\pi, \pi]$ sets the ellipticity of the waves. Special settings are linear polarization $\eta \in \{0, \pi\}$ and circular polarization $\eta = \pm\pi/2$.

A slight modification, namely the removal of $\pm$ in front of η, causes the waves to have equal helicity:

$$\boldsymbol{E}_{1,2}^{\zeta\zeta} = \hat{E} \begin{pmatrix} 0 \\ \cos(kx \mp \omega t) \\ \cos(kx \mp \omega t + \eta) \end{pmatrix}, \tag{2.23a}$$

$$\boldsymbol{B}_{1,2}^{\zeta\zeta} = \frac{\hat{E}}{c} \begin{pmatrix} 0 \\ \mp\cos(kx \mp \omega t + \eta) \\ \pm\cos(kx \mp \omega t) \end{pmatrix}. \tag{2.23b}$$

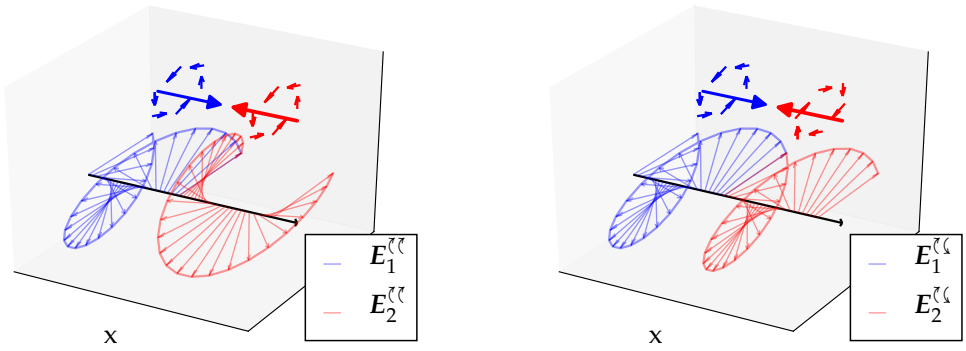

(a) opposite helicity (b) equal helicity

Figure 2.1: Visualization of the two different setups at circular polarization. The arrows around the black axis represent the respective electric field at a given time over a wavelength. The direction of propagation of the two different waves is displayed by the thick arrows above which are encircled by smaller arrows. These smaller arrows indicate the sense of rotation of the electric fields at a fixed position over time.

The difference between both cases is substantial. While the fields with opposite helicity have the same sense of rotation, the fields with equal helicity rotate in reverse directions at a fixed position over time. A graphical comparison of the two cases is depicted in figure 2.1. The superposition of the fields yields for opposite helicity

$$\boldsymbol{E}^{\curvearrowright\curvearrowright} = \boldsymbol{E}_1^{\curvearrowright\curvearrowright} + \boldsymbol{E}_2^{\curvearrowright\curvearrowright} = 2\hat{E}\cos(kx)\begin{pmatrix}0\\ \cos(\omega t)\\ \cos(\omega t-\eta)\end{pmatrix}, \tag{2.24a}$$

$$\boldsymbol{B}^{\curvearrowright\curvearrowright} = \boldsymbol{B}_1^{\curvearrowright\curvearrowright} + \boldsymbol{B}_2^{\curvearrowright\curvearrowright} = 2\frac{\hat{E}}{c}\sin(kx)\begin{pmatrix}0\\ -\sin(\omega t-\eta)\\ \sin(\omega t)\end{pmatrix} \tag{2.24b}$$

and for equal helicity

$$\boldsymbol{E}^{\curvearrowright\curvearrowleft} = \boldsymbol{E}_1^{\curvearrowright\curvearrowleft} + \boldsymbol{E}_2^{\curvearrowright\curvearrowleft} = 2\hat{E}\cos(\omega t)\begin{pmatrix}0\\ \cos(kx)\\ \cos(kx+\eta)\end{pmatrix}, \tag{2.25a}$$

$$\boldsymbol{B}^{\curvearrowright\curvearrowleft} = \boldsymbol{B}_1^{\curvearrowright\curvearrowleft} + \boldsymbol{B}_2^{\curvearrowright\curvearrowleft} = 2\frac{\hat{E}}{c}\sin(\omega t)\begin{pmatrix}0\\ -\sin(kx+\eta)\\ \sin(kx)\end{pmatrix}. \tag{2.25b}$$

In Coulomb gauge (transverse gauge, defined by $\nabla\boldsymbol{A} = 0$) the individual vector potentials

and the corresponding superposition are for opposite helicity

$$\boldsymbol{A}^{\circlearrowright\circlearrowright}_{1,2} = \pm\frac{\hat{E}}{\omega}\begin{pmatrix} 0 \\ \sin(kx \mp \omega t) \\ \sin(kx \mp \omega t \pm \eta) \end{pmatrix}, \tag{2.26a}$$

$$\boldsymbol{A}^{\circlearrowright\circlearrowright} = \boldsymbol{A}^{\circlearrowright\circlearrowright}_1 + \boldsymbol{A}^{\circlearrowright\circlearrowright}_2 = -\frac{2\hat{E}}{\omega}\cos(kx)\begin{pmatrix} 0 \\ \sin(\omega t) \\ \sin(\omega t - \eta) \end{pmatrix} \tag{2.26b}$$

and for equal helicity

$$\boldsymbol{A}^{\circlearrowright\circlearrowleft}_{1,2} = \pm\frac{\hat{E}}{\omega}\begin{pmatrix} 0 \\ \sin(kx \mp \omega t) \\ \sin(kx \mp \omega t + \eta) \end{pmatrix}, \tag{2.27a}$$

$$\boldsymbol{A}^{\circlearrowright\circlearrowleft} = \boldsymbol{A}^{\circlearrowright\circlearrowleft}_1 + \boldsymbol{A}^{\circlearrowright\circlearrowleft}_2 = -\frac{2\hat{E}}{\omega}\sin(\omega t)\begin{pmatrix} 0 \\ \cos(kx) \\ \cos(kx + \eta) \end{pmatrix} \tag{2.27b}$$

where $\boldsymbol{E} = -\frac{\partial \boldsymbol{A}}{\partial t}$ and $\boldsymbol{B} = \nabla \times \boldsymbol{A}$ with zero scalar potential. Note that $\boldsymbol{A}^{\circlearrowright\circlearrowright}$ and $\boldsymbol{A}^{\circlearrowright\circlearrowleft}$ describe exactly the same system in the limit of linear polarization.

2.6 Turn on

In the simulations the electromagnetic fields described in section 2.5 are modified by the window function

$$W(t) = \begin{cases} \sin^2(\frac{\pi t}{2\Delta T}) & \text{if } 0 \le t \le \Delta T, \\ 1 & \text{if } \Delta T \le t \le T - \Delta T, \\ \sin^2(\frac{\pi(T-t)}{2\Delta T}) & \text{if } T - \Delta T \le t \le T, \end{cases} \tag{2.28}$$

in which ΔT is the duration of a turn on/off and T is the interaction time. By means of this window function the light fields can be smoothly turned on and off. This modification is not without flaws. Please take a look at the following Maxwell equation also known as Maxwell-Faraday equation:

$$\nabla \times \boldsymbol{E} + \frac{\partial \boldsymbol{B}}{\partial t} = 0. \tag{2.29}$$

The plane wave fields of section 2.5 satisfy this equation. But the addition of the window function causes the second term in this equation to yield an additional term due to the time derivative. This term is by no means canceled by the first term. Therefore such a field that is switched on or off everywhere at the same time cannot exist in nature. Nevertheless, it can exist locally and hence it is applicable on a localized particle with a negligible error.

2.7 Initial condition and algorithm

The evolution of one electron in the light fields defined in section 2.5 is simulated for different parameters. In doing so, some simplifications are made. The physical system has a certain symmetry. The electromagnetic fields only depend on one space coordinate x and the electron momentum can only exchange discrete photon momenta in a direction parallel to the x-axis. Therefore this physical system can be modeled in one dimension. This means that the electron only moves along the x-axis but the fields acting on it are still three-dimensional. The electron is described by a basis of plane waves

$$\psi \propto \sum_{n,\gamma} c_n^\gamma \psi_n^\gamma =, \quad \gamma \in \{+\uparrow, +\downarrow, -\uparrow, -\downarrow\}, \tag{2.30}$$

in which ψ_n^γ are the plane wave solutions (2.9) but with discrete momenta $\boldsymbol{p} = nk\boldsymbol{e}_x$, $n \in \mathbb{Z}$ where k is the wave number of the light and $\boldsymbol{e}_x$ is the unit vector in the x-direction. Another simplification is that the fields are assumed to be independent of the presence of the electron and independent of any other effects.

In all simulations in the sections 3.1 and 4.1 the initial state is always such that the resonance condition (2.18) for the 2-photon Kapitza-Dirac effect is fulfilled. Furthermore, the spin up spinor is chosen as initial state. In terms of the coefficients c_n^γ in (2.30) this translates into $c_1^{+\uparrow} = 1$ while all other coefficients are zero.

The underlying algorithm of the simulations makes use of the Fourier split operator method [16] and the C++ library Q-Wave. The algorithm computes the time evolution of the wave function according to the Dirac equation which has the form

$$i\frac{\partial \psi}{\partial t} = \hat{\boldsymbol{H}}\psi. \tag{2.31}$$

The time evolution of the wave function ψ is given by

$$\psi(t) = \hat{\boldsymbol{U}}(t, t_0)\psi(t_0), \tag{2.32a}$$

$$\hat{\boldsymbol{U}}(t, t_0) = \hat{\boldsymbol{T}} \exp\left(-i \int_{t_0}^{t} \hat{\boldsymbol{H}}(\tau) \mathrm{d}\tau\right) \tag{2.32b}$$

with the time evolution operator $\hat{\boldsymbol{U}}$ and the time ordering operator $\hat{\boldsymbol{T}}$ [17]. For easy physical systems this expression can be calculated explicitly. If an analytical solution proves too difficult, numerical methods have to be used. The Fourier split operator method is one such method. The key feature of this method is the splitting of the operator $\hat{\boldsymbol{H}}$ into parts

$$\hat{\boldsymbol{H}} = \hat{\boldsymbol{T}} + \hat{\boldsymbol{V}} \tag{2.33}$$

that are diagonal either in momentum space ($\hat{\boldsymbol{T}}$) or in position space ($\hat{\boldsymbol{V}}$). In the case of the Dirac equation the Hamiltonian can be split into a free part

$$\hat{\boldsymbol{T}} = c\boldsymbol{\alpha} \cdot (\hat{\boldsymbol{p}}) + mc^2\boldsymbol{\beta} \tag{2.34}$$

and an interaction part

$$\hat{\boldsymbol{V}} = -cq\boldsymbol{\alpha} \cdot \boldsymbol{A} + q\Phi. \tag{2.35}$$

The time evolution operator $\hat{\boldsymbol{U}}$ (2.32a) can then be approximated by the following expansion

$$\begin{aligned}&\hat{\boldsymbol{U}}(t+\Delta t, t) = \\ &\exp\left(-\frac{i}{2}\int_t^{t+\Delta t} \hat{\boldsymbol{V}}(\tau)\mathrm{d}\tau\right)\exp\left(-i\int_t^{t+\Delta t} \hat{\boldsymbol{T}}(\tau)\mathrm{d}\tau\right)\exp\left(-\frac{i}{2}\int_t^{t+\Delta t} \hat{\boldsymbol{V}}(\tau)\mathrm{d}\tau\right) + O(\Delta t^3),\end{aligned} \tag{2.36}$$

and one time step Δt of the wave function can be calculated by [16]

$$\begin{aligned}\psi(t+\Delta t) = &\exp\left(-\frac{i}{2}\int_t^{t+\Delta t} \hat{\boldsymbol{V}}(\tau)\mathrm{d}\tau\right) \\ &\mathcal{F}^{-1}\left[\mathcal{F}\left[\exp\left(-i\int_t^{t+\Delta t} \hat{\boldsymbol{T}}(\tau)\mathrm{d}\tau\right)\right]\mathcal{F}\left[\exp\left(-\frac{i}{2}\int_t^{t+\Delta t} \hat{\boldsymbol{V}}(\tau)\mathrm{d}\tau\right)\psi(t)\right]\right],\end{aligned} \tag{2.37}$$

in which $\mathcal{F}$ denotes the Fourier transformation and $\mathcal{F}^{-1}$ the inverse Fourier transformation. Fourier transformations have to be performed in each time step. The advantage is that the operators become simple in their respective space. This scheme is of use for many partial differential equations, for instance, the nonlinear Schrödinger equation [18].

3 Kapitza-Dirac effect with counterrotating fields

3.1 Numerical results for counterrotating fields

The case of counterrotating fields corresponding to the vector potential $A^{\zeta\zeta}$ (2.27b) is simple because the evolution of the system is pretty much the same as the well understood two-photon Kapitza-Dirac effect for linear polarization. Essentially, the system oscillates back and forth between the two states corresponding to $c_1^{\uparrow}$ and $c_{-1}^{\uparrow}$. The probabilities of the respective modes, that is the scattering probabilities, evolve as follows

$$|c_1|^2 := |c_1^{+\uparrow}|^2 + |c_1^{+\downarrow}|^2 + |c_1^{-\uparrow}|^2 + |c_1^{-\downarrow}|^2 = \cos^2(\omega_R t), \tag{3.1}$$

$$|c_{-1}|^2 := |c_{-1}^{+\uparrow}|^2 + |c_{-1}^{+\downarrow}|^2 + |c_{-1}^{-\uparrow}|^2 + |c_{-1}^{-\downarrow}|^2 = \sin^2(\omega_R t) \tag{3.2}$$

$$|c_n|^2 \approx 0, \text{ for } |n| \neq 1 \tag{3.3}$$

which is shown in figure 3.1. Such cyclic behaviour between two quantum states is called Rabi flopping, one oscillation period is called Rabi cycle. The Rabi frequency ω_R for linear polarization is [7]

$$\omega_{\mathrm{R}}|_{\eta=0} = \frac{q^2\hat{E}^2}{2m\omega^2}. \tag{3.4}$$

The numerical results indicate that the elliptical polarization leads to an additional feature. The Rabi flopping gets more and more inhibited the more circularly polarized the light fields are. More precisely, the Rabi frequency ω_R is proportional to $\cos(\eta)$

$$\omega_{\mathrm{R}} = \frac{q^2\hat{E}^2}{2m\omega^2}\cos(\eta) \tag{3.5}$$

as shown in figure 3.2. For light of circular polarization ($\eta = \pi/2$) no Rabi flopping at all can be seen in the simulations.

3.2 Theory for counterrotating fields

3.2.1 From Dirac to Schrödinger

The following sections give a theoretical explanation for the numerical results found in section 3.1 which covers the Kapitza-Dirac effect with counterrotating fields. In

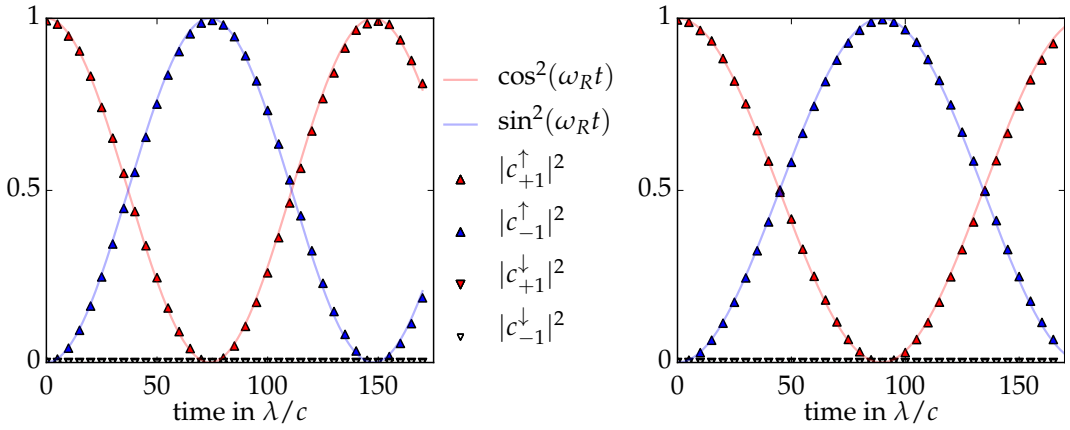

(a) linear polarization $\eta = 0$ (b) elliptical polarization $\eta = 0.6$

Figure 3.1: Rabi flopping for two different ellipticities. The light parameters are $\hat{E} = 400$ a.u. and $\lambda = 3$ a.u..

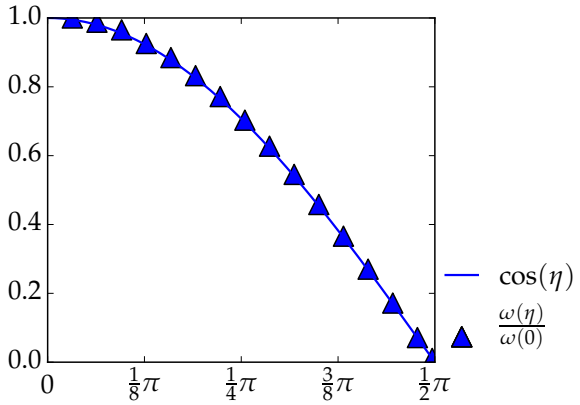

Figure 3.2: Numerical results for the Rabi frequency ω_R in the two-photon Kapitza-Dirac effect in the case of counterrotating fields (2.27b) as a function of ellipticity η normalized to the frequency for linearly polarized light. The light parameters are $\hat{E} = 400$ a.u. and $\lambda = 3$ a.u..

the simulations the fully relativistic Dirac equation is used. As the electron velocity is small compared to the speed of light in the studied parameter regime, it seems justified to consider the Foldy-Wouthuysen transformed Dirac Hamiltonian introduced in section 2.2.

$$i\frac{\partial\psi}{\partial t} = \Bigg[\frac{1}{2m}\left(\hat{\boldsymbol{p}} - q\boldsymbol{A}\right)^2 - \frac{q}{2m}\boldsymbol{B}\cdot\boldsymbol{\sigma} - \frac{q}{4m^2c^2}\boldsymbol{\sigma}\cdot\left(\boldsymbol{E}\times\left(\hat{\boldsymbol{p}} - q\boldsymbol{A}\right)\right) + mc^2 + q\Phi - \frac{q}{8m^2c^2}\nabla\boldsymbol{E} - \frac{1}{8m^3c^2}\left(\hat{\boldsymbol{p}} - q\boldsymbol{A}\right)^4 + \frac{q^2}{8m^3c^4}\left(\boldsymbol{E}^2 - c^2\boldsymbol{B}^2\right) + \frac{q}{8m^3c^2}\left\{\left(\hat{\boldsymbol{p}} - q\boldsymbol{A}\right)^2, \boldsymbol{B}\cdot\boldsymbol{\sigma}\right\}\Bigg]\psi \quad (3.6)$$

Essentially, this is the Pauli equation with some relativistic corrections. The Hamiltonian in this wave equation consists of many terms. Some are negligible, some vanish altogether. The last three terms that represent relativistic corrections to the kinetic energy, the electromagnetic fields and the spin coupling

$$-\frac{1}{8m^3c^2}\left(\hat{\boldsymbol{p}} - q\boldsymbol{A}\right)^4 + \frac{q^2}{8m^3c^4}\left(\boldsymbol{E}^2 - c^2\boldsymbol{B}^2\right) + \frac{q}{8m^3c^2}\left\{\left(\hat{\boldsymbol{p}} - q\boldsymbol{A}\right)^2, \boldsymbol{B}\cdot\boldsymbol{\sigma}\right\} \quad (3.7)$$

are negligible because they are three orders of magnitude lower compared to the first kinetic term in the studied parameter regime. These approximations are only valid if the inequalities

$$|\boldsymbol{p} - q\boldsymbol{A}| \ll mc, \quad \frac{|q\boldsymbol{E}|}{|\boldsymbol{p} - q\boldsymbol{A}|} \ll mc^2, \quad |q\boldsymbol{E}| \ll m^2c^3 \quad (3.8)$$

hold. This means that the electron must not be too fast and the fields not too strong. As the divergence of the electric field (2.25a) is zero, the term proportional to $\nabla\boldsymbol{E}$ vanishes likewise. Furthermore, the scalar potential ϕ is zero and the term mc^2 can be canceled by gauge freedom:

$$\begin{aligned} i\frac{\partial\psi}{\partial t} &= \left[\frac{1}{2m}(\hat{\boldsymbol{p}} - q\boldsymbol{A})^2 - \frac{q}{2m}\boldsymbol{B}\cdot\boldsymbol{\sigma} - \frac{q}{4m^2c^2}\boldsymbol{\sigma}\cdot\left(\boldsymbol{E}\times\left(\hat{\boldsymbol{p}} - q\boldsymbol{A}\right)\right)\right]\psi \\ &= \left[\frac{1}{2m}\left(\hat{\boldsymbol{p}}^2 + q^2\boldsymbol{A}^2 + iq\nabla\boldsymbol{A} + 2iq\boldsymbol{A}\nabla\right) - \frac{q}{2m}\boldsymbol{B}\cdot\boldsymbol{\sigma} - \frac{q}{4m^2c^2}\boldsymbol{\sigma}\cdot\left(\boldsymbol{E}\times\hat{\boldsymbol{p}}\right) + \frac{q^2}{4m^2c^2}\boldsymbol{\sigma}\cdot\left(\boldsymbol{E}\times\boldsymbol{A}\right)\right]\psi. \end{aligned}$$

This differential equation can be further simplified. In Coulomb gauge the term $\propto \nabla\boldsymbol{A}$ is zero. The term right next to it that is proportional to $\boldsymbol{A}\nabla$ vanishes once a wave equation which depends only on x is inserted. The reason is that its gradient $\nabla\psi$ is in this case pependicular to $\boldsymbol{A}$ and hence the dot product between $\boldsymbol{A}$ and $\nabla\psi$ gets zero. The last term proportional to $\boldsymbol{E}\times\boldsymbol{A}$ couples the electron spin with the spin angular momentum of light (2.17). This term becomes zero in the case of counterrotating fields. It remains

$$i\frac{\partial\psi}{\partial t} = \left[\frac{1}{2m}\left(\hat{\boldsymbol{p}}^2 + q^2\boldsymbol{A}^2\right) - \frac{q}{2m}\boldsymbol{B}\cdot\boldsymbol{\sigma} - \frac{q}{4m^2c^2}\boldsymbol{\sigma}\cdot\left(\boldsymbol{E}\times\hat{\boldsymbol{p}}\right)\right]\psi \quad (3.9)$$

which consists of the remnants of the kinetic part and two spin terms. The first one, that is the Zeeman term, couples the electron spin to the magnetic field. The second term couples the electron spin to its momentum. In the case of the hydrogen atom, where the electron is in a radially symmetric scalar potential, this term leads to the famous spin-orbit coupling [10].

In order to get rid of the annoying time dependencies in the Hamiltonian, the next steps derive an approximated Hamiltonian by means of a Magnus expansion. The Magnus expansion gives a fundamental solution of

$$\dot{\boldsymbol{Y}}(t) = \boldsymbol{F}(t)\boldsymbol{Y}(t) \tag{3.10}$$

in terms of the exponential of a function $\Omega(t)$

$$\boldsymbol{Y}(t) = e^{\boldsymbol{\Omega}(t)}, \quad \boldsymbol{Y}(t_0) = \mathbf{1} \tag{3.11}$$

that is defined by an infinite series whose first terms are [19, 20]

$$\boldsymbol{\Omega}(t) = \int_0^t \boldsymbol{F}(t_1)\mathrm{d}t_1 + \frac{1}{2}\int_0^t \left(\int_0^{t_1} [\boldsymbol{F}(t_1), \boldsymbol{F}(t_2)]\,\mathrm{d}t_2\right)\mathrm{d}t_1 + \ldots. \tag{3.12}$$

The Magnus expansion is used in many fields [21] as an approximative method for the solution of differential equations. The approximation is done by a truncation of the infinite series above. In contrast to time dependent perturbation theory the Magnus expansion preserves the unitarity of a unitary operator after truncation at any order [22].

Let $\boldsymbol{F}(t)$ be the Hamiltonian in equation (4.13) divided by the imaginary unit from the left hand side of the equation (for having the same structure as in the definition (3.10)). With the Magnus expansion the approximative solution for equation (4.13) with initial value $\psi(t_0)$ reads

$$\psi(t) = \exp\left(\int_0^t \boldsymbol{F}(t_1)\mathrm{d}t_1 + \frac{1}{2}\int_0^t \left(\int_0^{t_1} [\boldsymbol{F}(t_1), \boldsymbol{F}(t_2)]\,\mathrm{d}t_2\right)\mathrm{d}t_1\right)\psi(t_0), \tag{3.13}$$

in which the infinite series is truncated after the second term as in (3.12). This yields a lot of terms that evolve differently in time. Most of them are bounded and feature an oscillatory time evolution but some are not bounded but grow linearly in time. In the long run, these linearly growing terms are the dominant terms. Therefore only those terms are kept. In doing so, an approximated Hamiltonian can be retrieved. The system can then be described by the Schrödinger equation with this approximated Hamiltonian

$$i\frac{\partial\psi}{\partial t} = \left[\frac{1}{2m}\hat{\boldsymbol{p}}^2 + \frac{q^2\hat{E}^2}{m\omega^2}\left(\cos^2(kx) + \cos^2(kx+\eta)\right)\right]\psi. \tag{3.14}$$

The spin parts vanish in this approximation and thus spin effects or effects related to coupling of angular momenta are therefore without effect.

This can be understood by the following considerations. The time dependency of the electromagnetic fields $\boldsymbol{E}^{(\zeta)}$ (2.25a) and $\boldsymbol{B}^{(\zeta)}$ (2.25b) is a global phase. They do not rotate

around the x-axis and their spatial shape stays constant. Only their amplitude oscillates swiftly according to $\cos(\omega t)$. The spin parts therefore change their sign constantly over and over again much faster than the electron can react to it. This means that the movement of the electron is not in phase with them and over long periods of time spin effects are bounded and very small. The individual spinor components of the wave function are therefore decoupled.

The potential in equation (3.14) comes from the kinetic part which is proportional to A^2. This potential can also be derived by averaging the kinetic term in equation (3.9) over time. In essence, this is what happens in the Magnus expansion here. Such time averaged potentials, called ponderomotive potentials, are often of use for describing the trajectory of particles in fast oscillating fields. The reason is that in such cases the trajectory of the particle can be split up into a smooth trajectory and a negligible oscillatory perturbation around that smooth trajectory. One can show [23] that the smooth trajectory is completely governed by a ponderomotive potential.

3.2.2 Simplifying the ponderomotive potential

The ponderomotive potential

$$V_{\text{pond}}^{\mathbb{C}\ell} = \frac{q^2\hat{E}^2}{m\omega^2}(\cos^2(kx) + \cos^2(kx+\eta)) \tag{3.15}$$

can be rewritten by means of a little algebra and coordinate/gauge transformations. Applying the identity

$$\begin{aligned}
&\cos^2(x) + \cos^2(x+\eta) \\
&= \frac{1}{4}\left(4 + e^{2i\eta}e^{2ix} + e^{2ix} + e^{-2ix} + e^{-2i\eta}e^{-2ix}\right) \\
&= \frac{1}{4}\left(4 + (e^{i\eta} + e^{-i\eta})(e^{i(2x+\eta)} + e^{-i(2x+\eta)})\right) \\
&= \frac{1}{4}\left(4 + 2\cos(\eta)((e^{i(x+\eta/2)} + e^{-i(x-\eta/2)})^2 - 2)\right) \\
&= 2\cos(\eta)\cos^2(x+\eta/2) + (1-\cos(\eta))
\end{aligned} \tag{3.16}$$

to (3.15) yields

$$V^{\mathbb{C}\ell} = \frac{q^2\hat{E}^2}{m\omega^2}\left(2\cos(\eta)\cos^2(kx+\eta/2) + (1-\cos(\eta))\right). \tag{3.17}$$

Potentials are not observable, only the corresponding forces are observable. Adding a suitable constant to $V^{\mathbb{C}\ell}$ does not change the resulting force but makes the potential easier. One can further simplify $V^{\mathbb{C}\ell}$ by the coordinate transformation $kx \to kx' = kx - \eta/2$ as follows

$$V^{\mathbb{C}\ell} = \frac{2q^2\hat{E}^2}{m\omega^2}\cos(\eta)\cos^2(kx'). \tag{3.18}$$

This coordinate transformation does not change the physical system because it is totally symmetric in the x-direction. Therefore, the prime in x' will be omitted in the following section. The amplitude of the ponderomotive potential is proportional to $\cos(\eta)$ and in particular vanishes for circular polarization ($\eta = \pm\pi/2$) as does the resulting force. This suggests that no reflections occur for circular polarization.

3.2.3 Solving the Schrödinger equation

In this section the Schrödinger equation (3.14) with the simplified ponderomotive potential (3.18) is solved. In doing so, the plane wave ansatz

$$\psi = \sum_{n=-\infty}^{\infty} \boldsymbol{c}_n(t) e^{iknx} \tag{3.19}$$

is inserted into the Schrödinger equation:

$$\begin{aligned}
&i \sum_n \dot{\boldsymbol{c}}_n(t) e^{iknx} \\
&= \sum_n \left(-\frac{1}{2m} \frac{\partial^2}{\partial x^2} \boldsymbol{c}_n(t) e^{iknx} + \frac{2q^2E^2}{m\omega^2} \cos(\eta) \left(\frac{1}{2} \left(e^{ikx} + e^{-ikx} \right) \right)^2 \boldsymbol{c}_n(t) e^{iknx} \right) \\
&= \sum_n \left(\frac{k^2n^2}{2m} \boldsymbol{c}_n(t) e^{iknx} + \frac{q^2E^2}{2m\omega^2} \cos(\eta) \left(\boldsymbol{c}_n(t) e^{ik(n+2)x} + 2\boldsymbol{c}_n(t) e^{iknx} + \boldsymbol{c}_n(t) e^{ik(n-2)x} \right) \right),
\end{aligned}$$

whence by equating coefficients one obtains a system of coupled ordinary differential equations for the time dependent coefficients $\boldsymbol{c}_n(t)$

$$i\dot{\boldsymbol{c}}_n(t) = \left(\frac{k^2n^2}{2m} + \frac{q^2E^2}{m\omega^2} \cos(\eta) \right) \boldsymbol{c}_n(t) + \frac{q^2E^2}{2m\omega^2} \cos(\eta) \left(\boldsymbol{c}_{n-2}(t) + \boldsymbol{c}_{n+2}(t) \right), \tag{3.20}$$

in which even modes couple only with even modes and odd modes couple only with odd modes. The individual spin components of $\boldsymbol{c}$ are completely decoupled. If the odd mode $c_1^{\uparrow}(t = 0) = 1$ is fully populated initially, probability can only flow along the neighbouring odd modes with spin up. But as the kinetic energy grows quadratically with n, the coupling with the modes of higher n is supressed. Therefore the linear system can be truncated at a certain mode. This is only valid if the kinetic part itself is not smaller than the field terms [7], that is to say, the field strength and the wavelength of the light must not be too large. With the abbreviations

$$\varepsilon(n) := \frac{k^2n^2}{2m} + \frac{q^2E^2}{m\omega^2} \cos(\eta), \quad \varepsilon := \varepsilon(1) = \varepsilon(-1) \tag{3.21}$$

$$\omega_{\mathrm{R}} := \frac{q^2E^2}{2m\omega^2} \cos(\eta) \tag{3.22}$$

the linear system truncated to the first modes reads

$$i\begin{pmatrix}\dot{c}_1(t)\\ \dot{c}_{-1}(t)\end{pmatrix} = \begin{pmatrix}\varepsilon & \omega_\mathrm{R}\\ \omega_\mathrm{R} & \varepsilon\end{pmatrix}\begin{pmatrix}c_1(t)\\ c_{-1}(t)\end{pmatrix} \tag{3.23}$$

$$= \begin{pmatrix}-1 & 1\\ 1 & 1\end{pmatrix}\begin{pmatrix}\varepsilon-\omega_\mathrm{R} & 0\\ 0 & \varepsilon+\omega_\mathrm{R}\end{pmatrix}\begin{pmatrix}-1/2 & 1/2\\ 1/2 & 1/2\end{pmatrix}\begin{pmatrix}c_1(t)\\ c_{-1}(t)\end{pmatrix}. \tag{3.24}$$

The solution of the linear system is therefore

$$\begin{pmatrix}c_1(t)\\ c_{-1}(t)\end{pmatrix} = \kappa_1\begin{pmatrix}-1\\ 1\end{pmatrix}e^{-i(\varepsilon-\omega_\mathrm{R})t} + \kappa_2\begin{pmatrix}1\\ 1\end{pmatrix}e^{-i(\varepsilon+\omega_\mathrm{R})t} \tag{3.25}$$

with yet to be determined coefficients κ_1 and κ_2. From the initial value problem

$$\begin{pmatrix}c_1(t_0)\\ c_{-1}(t_0)\end{pmatrix} := \begin{pmatrix}c_1(0)\\ c_{-1}(0)\end{pmatrix} = \begin{pmatrix}1\\ 0\end{pmatrix}, \tag{3.26}$$

which represents the initial state, one obtains $\kappa_1 = -\kappa_2 = 1/2$. The insertion into the general solution (3.25) yields

$$\begin{pmatrix}c_1(t)\\ c_{-1}(t)\end{pmatrix} = \frac{e^{-i\varepsilon t}}{2}\begin{pmatrix}e^{\omega_\mathrm{R}t}+e^{-\omega_\mathrm{R}t}\\ -e^{\omega_\mathrm{R}t}+e^{-\omega_\mathrm{R}t}\end{pmatrix} = e^{-i\varepsilon t}\begin{pmatrix}\cos(\omega_\mathrm{R}t)\\ -\cos(\omega_\mathrm{R}t)\end{pmatrix}, \tag{3.27}$$

and the physically more interesting squared absolute values

$$\begin{pmatrix}|c_1(t)|^2\\ |c_{-1}(t)|^2\end{pmatrix} = \begin{pmatrix}\cos^2(\omega_\mathrm{R}t)\\ \sin^2(\omega_\mathrm{R}t)\end{pmatrix}, \quad \omega_R = \frac{q^2E^2}{2m\omega^2}\cos(\eta). \tag{3.28}$$

This is in agreement with the numerical results and in particular with the dependency of the Rabi frequency on η. Note that such calculations have been carried out by other people [3] [7] too for linearly polarized light fields.

4 Kapitza-Dirac effect with corotating fields

4.1 Numerical results for corotating fields

The case of corotating fields corresponding to the vector potential $\boldsymbol{A}^{\circlearrowleft\circlearrowleft}$ (2.26b) produces a more complex behaviour as compared to section 3.1. In this case it is useful to distinguish different time scales. For a short interaction time such as some Rabi cycles the evolution is similar to that of linear polarization. Rabi flopping occurs between the two modes $c_1^{+\uparrow}$ and $c_{-1}^{+\uparrow}$ with no dependency of the Rabi frequency ω_R on η at all. In this time scale no spin effects are visible.

For longer interaction times spin effects do become visible as can be seen in figure 4.1. The spin expectation value

$$\langle s_z \rangle = \frac{1}{2} \sum_n |c_n^{+\uparrow}|^2 - |c_n^{+\downarrow}|^2 + |c_n^{-\uparrow}|^2 - |c_n^{-\downarrow}|^2 \tag{4.1}$$

oscillates around the optical axis and can in this time scale written as

$$\langle s_z \rangle = \frac{1}{2} \cos(\omega_{\text{fast}} t) \tag{4.2}$$

with a frequency ω_{fast}. The time evolution of the coefficients $c_n^{\gamma}(t)$

$$|c_1^{+\uparrow}| = \cos^2(\frac{\omega_{\text{fast}}}{2} t) \cos^2(\omega_{\text{R}} t) \tag{4.3}$$

$$|c_1^{+\downarrow}| = \sin^2(\frac{\omega_{\text{fast}}}{2} t) \cos^2(\omega_{\text{R}} t) \tag{4.4}$$

$$|c_{-1}^{+\uparrow}| = \cos^2(\frac{\omega_{\text{fast}}}{2} t) \sin^2(\omega_{\text{R}} t) \tag{4.5}$$

$$|c_{-1}^{+\downarrow}| = \sin^2(\frac{\omega_{\text{fast}}}{2} t) \sin^2(\omega_{\text{R}} t) \tag{4.6}$$

$$\tag{4.7}$$

reflects this behaviour. But this again is only valid for certain time scale. For even longer interaction times the spin expectation value $\langle s_z \rangle$ gets an envelope

$$\langle s_z \rangle = \frac{1}{2} \cos(\omega_{\text{fast}} t) \cos(\omega_{\text{slow}} t) \tag{4.8}$$

with a frequency ω_{slow}.

In order to find out more about the spin dynamics, the data describing $\langle s_z \rangle$ has been fitted using the function (4.8) for several parameters. Both the fast spin oscillation

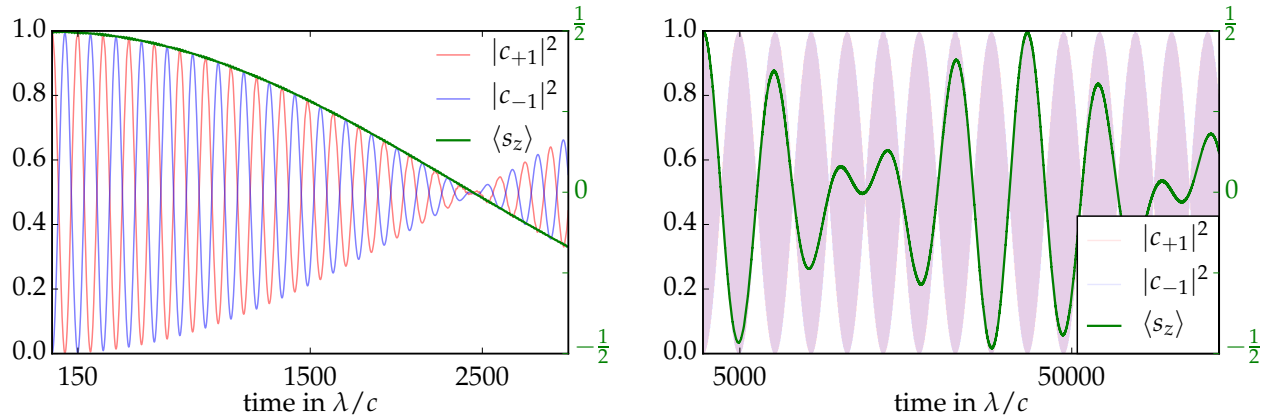

(a) intermediate timescale

(b) long timescale

Figure 4.1: Time evolution of the spin expectation value and the scattering probabilities $|c_{+1}|^2$, $|c_{-1}|^2$ as defined in 3.1 for two different time scales and circularly polarized light in the case of corotating fields. The light parameters are $\hat{E} = 400$ a.u. and $\lambda = 3$ a.u..

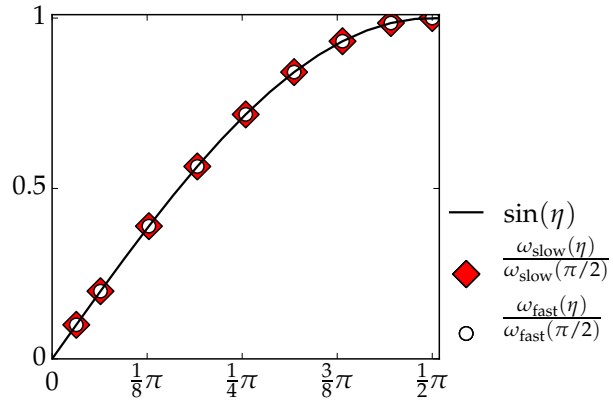

Figure 4.2: Both spin frequencies as a function of ellipticity η in the case of corotating fields normalized to the frequency for circularly polarized light ($\eta = \pi/2$). The light parameters are $\hat{E} = 400$ a.u. and $\lambda = 3$ a.u..

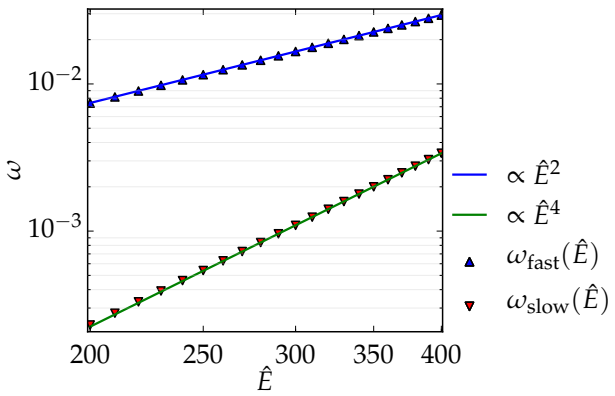

Figure 4.3: Both spin frequencies ω_{fast} and ω_{slow} for different electric field strenghts at circular polarization in the case of corotating fields ((2.26b)). The wavelength is $\lambda = 3$ a.u..

frequency ω_{fast} and the slower spin frequency ω_{slow} are proportional to $\sin(\eta)$ as shown in figure 4.2. While the slow spin frequency grows with the fourth power of the electric field strength, the fast spin frequency grows only quadratically (see figure 4.3). The dependency of the fast frequency on the wave length of the light is a plain linear law as depicted in figure 4.4(a).

The slow frequency is a little more interesting because a power law fails for small wave lengths in the studied parameter range. An exponential law describes the data much better in this regime. In the regime of larger wave lengths the slow frequency ω_{slow} appears to be proportional to the fifth power of the wave length as shown in figure 4.4(b). All results for the fast spin precession frequency put together yield

$$\omega_{\text{fast}} = \frac{\hat{E}^2 \lambda \sin \eta}{2\pi c^3}. \tag{4.9}$$

In the regime of long wavelengths

$$\omega_{\text{slow}} = \frac{\hat{E}^4 \lambda^5 \sin \eta}{4\,(2\pi c)^5} \tag{4.10}$$

describes the slow spin precession frequency quite well. Both proportionality constants were found empirically.

The choice of a suitable parameter range for the light parameters $\hat{E}$ or λ is a trade-off between two factors. The first factor sets an upper limit on the parameters. If the wavelength or the electric field strength (intensity) are too big, the system exhibits chaotic behaviour. The second factor is simulation time and sets a lower limit on these parameters. The necessary simulation time to make these spin effects visible grows very fast as the mentioned parameters get smaller.

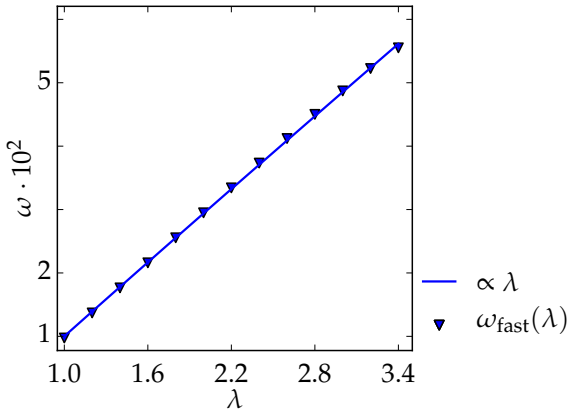

(a) Fast spin frequency ω_{fast}

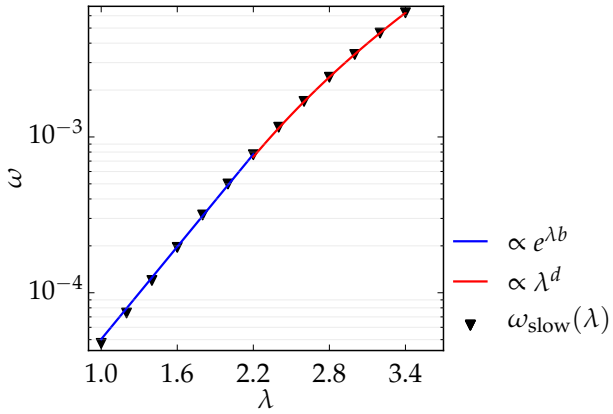

(b) Slow spin frequency ω_{slow}

Figure 4.4: Both spin frequencies versus wavelength at circular polarization for the case of corotating fields. The electric field strength is $\hat{E} = 400$ a.u.. The lines are fits. For the slow spin frequency the fits in the respective regimes yield d ≈ 4.9 and b ≈ 2.3.

4.2 Theory for corotating fields

4.2.1 From Dirac to Pauli

This section follows the same approach made in section 3.2.1, namely an approximation of the Foldy-Wouthuysen transformed Dirac equation

$$i\frac{\partial\psi}{\partial t} = \Bigg[\frac{1}{2m}(\hat{\boldsymbol{p}} - q\boldsymbol{A})^2 - \frac{q}{2m}\boldsymbol{B}\cdot\boldsymbol{\sigma} - \frac{q}{4m^2c^2}\boldsymbol{\sigma}\cdot(\boldsymbol{E}\times(\hat{\boldsymbol{p}} - q\boldsymbol{A})) + mc^2 + q\Phi - \frac{q}{8m^2c^2}\nabla\boldsymbol{E} - \frac{1}{8m^3c^2}(\hat{\boldsymbol{p}} - q\boldsymbol{A})^4 + \frac{q^2}{8m^3c^4}\left(\boldsymbol{E}^2 - c^2\boldsymbol{B}^2\right) + \frac{q}{8m^3c^2}\left\{(\hat{\boldsymbol{p}} - q\boldsymbol{A})^2, \boldsymbol{B}\cdot\boldsymbol{\sigma}\right\}\Bigg]\psi \quad (4.11)$$

in order to obtain a simple wave equation. The first steps are the same as in section 3.2.1. The last six terms and some parts of the kinetic term are neglected because they either vanish, are very small compared to the other terms or can be canceled by a suitable regauge. It remains a Pauli equation

$$i\frac{\partial\psi}{\partial t} = \left[\frac{1}{2m}\left(\hat{\boldsymbol{p}}^2 + q^2\boldsymbol{A}^2\right) - \frac{q}{2m}\boldsymbol{B}\cdot\boldsymbol{\sigma} - \frac{q}{4m^2c^2}\boldsymbol{\sigma}\cdot(\boldsymbol{E}\times(\hat{\boldsymbol{p}} - q\boldsymbol{A}))\right]\psi \quad (4.12)$$

with some relativistic spin corrections. The term that is proportional to the spin density (2.17) vanishes directly in the counterrotating case and the other spin terms are without

effect in that case. Though this time the spin density and the effect of the other spin terms do not vanish. This is due to the electromagnetic fields that feature a completely different behaviour as compared to the fields in the counterrotating case. In essence, the corotating fields rotate around the optical axis in contrast to the counterrotating fields which merely have an oscillating amplitude. In the following exactly the same strategy as in section 3.2.1 is used. At first, the electromagnetic fields (2.24a) (2.24b) (2.26b) are inserted into equation (4.12)

$$\begin{aligned} i\frac{\partial\psi}{\partial t} = \Bigg[& \frac{1}{2m}\hat{\boldsymbol{p}}^2 + \frac{q^2}{2m}\boldsymbol{A}^2 - \frac{q}{2m}\boldsymbol{B}\cdot\boldsymbol{\sigma} - \frac{qkn}{4m^2c^2}\boldsymbol{\sigma}\cdot(\boldsymbol{E}\times\boldsymbol{e}_x) + \frac{q^2}{4m^2c^2}\boldsymbol{E}\times\boldsymbol{A}\Bigg]\psi \\ & \Bigg[\frac{1}{2m}\hat{\boldsymbol{p}}^2 + \frac{2q^2\hat{E}^2}{m\omega^2}\cos^2(kx)\left(\sin^2(\omega t) + \sin^2(\omega t-\eta)\right) \\ & - \frac{q\hat{E}}{mc}\sin(kx)\left(-\sin(\omega t-\eta)\sigma_2 + \sin(\omega t)\sigma_3\right) \\ & - \frac{qn\omega\hat{E}}{2m^2c^3}\cos(kx)\left(\cos(\omega t-\eta)\sigma_2 - \cos(\omega t)\sigma_3\right) + \frac{q^2\hat{E}^2}{m^2c^2\omega}\sin(\eta)\cos^2(kx)\sigma_1\Bigg]\psi \end{aligned} \tag{4.13}$$

whose Hamiltonian is again approximated by means of a Magnus expansion that is truncated after the second term. A tedious calculation yields an approximated Hamiltonian which reads

$$\begin{aligned} i\frac{\partial\psi}{\partial t} = \Bigg[& \left(\frac{k^2n^2}{2m} + \frac{2q^2\hat{E}^2}{m\omega^2}\cos^2(kx)\right) \\ & + \Bigg(\frac{q^2\hat{E}^2\sin(\eta)}{m^2c^2\omega}\cos^2(kx) - \frac{q^2\hat{E}^2\sin(\eta)}{m^2c^2\omega}\sin^2(kx) \\ & - \frac{q^2\hat{E}^2n^2\omega\sin(\eta)}{4m^4c^6}\cos^2(kx)\Bigg)\sigma_1\Bigg]\psi, \end{aligned} \tag{4.14}$$

keeping again only the dominant terms. One of them

$$-\frac{q^2\hat{E}^2n^2\omega\sin(\eta)}{4m^4c^6}\cos^2(kx) \tag{4.15}$$

is very small but is kept because it grows significantly if the wavelength ($\omega \propto 1/\lambda$) is small or modes of big n are populated. Therefore it could be of influence in such cases. It is instructive to compare (4.14) with the approximation for counterrotating fields (3.9) and the results of the two simulation sections 3.1 4.1. The ponderomotive potential is here independent of η. This is the reason why the Rabi cycles are independent of ellipticity in this case. Furthermore, there are nonvanishing spin terms that depend on $\sin(\eta)$. This is certainly connected with the $\sin(\eta)$-laws (4.9)(4.10) that were found numerically for both spin frequencies. Additionally, there is a term that grows for small wavelengths. This one might be responsible for the odd behaviour of the slow spin frequency at small wavelengths.

4.2.2 Solving the Pauli equation

The insertion of the wave function

$$\psi = \sum_{n=-\infty}^{\infty} \boldsymbol{c}_n(t) e^{iknx} =: \sum_{n=-\infty}^{\infty} \psi_n \tag{4.16}$$

and expansion of all trigonometric functions that depend on x and equating coefficients as done in section 3.2.3 yields a system of coupled differential equations for the coefficients $\boldsymbol{c}_n(t)$

$$\begin{aligned} i\dot{\boldsymbol{c}}_n(t) = {} & \frac{k^2n^2}{2m}\boldsymbol{c}_n(t) + \frac{q^2\hat{E}^2}{2m\omega^2}\left(\boldsymbol{c}_{n-2}(t) + 2\boldsymbol{c}_n(t) + \boldsymbol{c}_{n+2}(t)\right) \\ & + \frac{q^2\hat{E}^2\sin(\eta)}{2m^2c^2\omega}\left(\boldsymbol{c}_{n-2}(t) + \boldsymbol{c}_{n+2}(t)\right)\sigma_1 - \frac{q^2\hat{E}^2n^2\omega\sin(\eta)}{16m^4c^6}\left(\boldsymbol{c}_{n-2}(t) + 2\boldsymbol{c}_n(t) + \boldsymbol{c}_{n+2}(t)\right)\sigma_1 \end{aligned} \tag{4.17}$$

which is equivalent to

$$\begin{aligned} i\dot{\boldsymbol{c}}_n(t) = {} & \left(\frac{k^2n^2}{2m} + \frac{q^2\hat{E}^2}{m\omega^2} - \frac{q^2\hat{E}^2n^2\omega\sin(\eta)}{8m^4c^6}\sigma_1\right)\boldsymbol{c}_n(t) \\ & + \left(\frac{q^2\hat{E}^2}{2m\omega^2} + \left(\frac{q^2\hat{E}^2\sin(\eta)}{2m^2c^2\omega} - \frac{q^2\hat{E}^2n^2\omega\sin(\eta)}{16m^4c^6}\right)\sigma_1\right)\left(\boldsymbol{c}_{n-2}(t) + \boldsymbol{c}_{n+2}(t)\right). \end{aligned} \tag{4.18}$$

Because the truncation to the first modes worked previously for the case of counterrotating fields let us assume that this is here justified too. With the abbreviations

$$\varepsilon(n) := \frac{k^2n^2}{2m} + \frac{q^2E^2}{m\omega^2}, \quad \varepsilon := \varepsilon(1) = \varepsilon(-1) \tag{4.19}$$

$$\omega_{\mathrm{R}} := \frac{q^2E^2}{2m\omega^2} \tag{4.20}$$

$$\omega_{\mathrm{fast}/2} := \frac{q^2\hat{E}^2\sin(\eta)}{2m^2c^2\omega} \tag{4.21}$$

$$\chi := \frac{q^2\hat{E}^2n^2\omega\sin(\eta)}{16m^4c^6} \tag{4.22}$$

the linear system truncated to the first modes reads

$$i\dot{\boldsymbol{c}} = \begin{pmatrix} \varepsilon + 2\omega_{\mathrm{R}} & -2\chi & \omega_{\mathrm{R}} & \omega_{\mathrm{fast}/2} - \chi \\ -2\chi & \varepsilon + 2\omega_{\mathrm{R}} & \omega_{\mathrm{fast}/2} - \chi & \omega_{\mathrm{R}} \\ \omega_{\mathrm{R}} & \omega_{\mathrm{fast}/2} - \chi & \varepsilon + 2\omega_{\mathrm{R}} & -2\chi \\ \omega_{\mathrm{fast}/2} - \chi & \omega_{\mathrm{R}} & -2\chi & \varepsilon + 2\omega_{\mathrm{R}} \end{pmatrix} \boldsymbol{c} = \boldsymbol{P}\boldsymbol{D}\boldsymbol{P}^{-1}\boldsymbol{c}, \tag{4.23}$$

in which

$$\boldsymbol{P} = \begin{pmatrix} 1 & 1 & 1 & 1 \\ -1 & -1 & 1 & 1 \\ -1 & 1 & 1 & -1 \\ 1 & -1 & 1 & -1 \end{pmatrix} \tag{4.24}$$

and $\boldsymbol{D}$ is a diagonal matrix with the entries

$$\boldsymbol{D}_{i,i} = \begin{pmatrix} \varepsilon + \omega_{\mathrm{R}} + \omega_{\mathrm{fast}/2} + \chi \\ \varepsilon + 3\omega_{\mathrm{R}} - \omega_{\mathrm{fast}/2} + 3\chi \\ \varepsilon + 3\omega_{\mathrm{R}} + \omega_{\mathrm{fast}/2} - 3\chi \\ \varepsilon + \omega_{\mathrm{R}} - \omega_{\mathrm{fast}/2} - \chi \end{pmatrix}. \tag{4.25}$$

The solution of the linear system for the initial condition $\boldsymbol{c}(0) = (1,0,0,0)^T$ is then

$$\begin{aligned} \boldsymbol{c}(t) = \frac{1}{4}\begin{pmatrix}1\\1\\1\\1\end{pmatrix} e^{-it(\varepsilon+\omega_{\mathrm{R}}+\omega_{\mathrm{fast}/2}+\chi)} + \frac{1}{4}\begin{pmatrix}1\\-1\\1\\-1\end{pmatrix} e^{-it(\varepsilon+3\omega_{\mathrm{R}}-\omega_{\mathrm{fast}/2}+3\chi)} \\ + \frac{1}{4}\begin{pmatrix}1\\1\\1\\1\end{pmatrix} e^{-it(\varepsilon+3\omega_{\mathrm{R}}+\omega_{\mathrm{fast}/2}-3\chi)} + \frac{1}{4}\begin{pmatrix}1\\1\\-1\\-1\end{pmatrix} e^{-it(\varepsilon+\omega_{\mathrm{R}}-\omega_{\mathrm{fast}/2}-\chi)}. \end{aligned} \tag{4.26}$$

If χ is neglected, the solution reads

$$\begin{pmatrix} c_1^{\uparrow} \\ c_1^{\downarrow} \\ c_{-1}^{\uparrow} \\ c_{-1}^{\downarrow} \end{pmatrix} = e^{-it(\varepsilon+2\omega_{\mathrm{R}})} \begin{pmatrix} \cos(\omega_{\mathrm{fast}/2}t)\cos(\omega_R t) \\ i\sin(\omega_{\mathrm{fast}/2}t)\cos(\omega_R t) \\ -i\cos(\omega_{\mathrm{fast}/2}t)\sin(\omega_R t) \\ -\sin(\omega_{\mathrm{fast}/2}t)\sin(\omega_R t), \end{pmatrix} \tag{4.27}$$

whence the squared absolute values of the coefficients

$$\begin{pmatrix} |c_1^{\uparrow}|^2 \\ |c_1^{\downarrow}|^2 \\ |c_{-1}^{\uparrow}|^2 \\ |c_{-1}^{\downarrow}|^2 \end{pmatrix} = \begin{pmatrix} \cos^2(\omega_{\mathrm{fast}/2}t)\cos^2(\omega_R t) \\ \sin^2(\omega_{\mathrm{fast}/2}t)\cos^2(\omega_R t) \\ \cos^2(\omega_{\mathrm{fast}/2}t)\sin^2(\omega_R t) \\ \sin^2(\omega_{\mathrm{fast}/2}t)\sin^2(\omega_R t) \end{pmatrix} \tag{4.28}$$

is obtained. The χ is neglected because it is very small and does not change the solution fundamentally. The spin expectation value is then

$$\langle s_z \rangle = \frac{1}{2}\left(\cos^2(\omega_{\mathrm{fast}/2}) - \sin^2(\omega_{\mathrm{fast}/2})\right) = \frac{1}{2}\cos(2\omega_{\mathrm{fast}/2}) = \frac{1}{2}\cos(\omega_{\mathrm{fast}}). \tag{4.29}$$

The solution is in agreement with the intermediate time evolution in the simulations (4.1) (4.3). But it is in disagreement with the long term behaviour (4.8). This is due to the truncation to the two modes $\boldsymbol{c}_1$, $\boldsymbol{c}_{-1}$. Although only very weakly populated, the modes $\boldsymbol{c}_3$, $\boldsymbol{c}_{-3}$ are of influence. A truncation of the linear system (4.18) after the modes $\boldsymbol{c}_3$, $\boldsymbol{c}_{-3}$ and omission of small terms (χ) yields a solution that features almost the same long term dynamic as found in the simulations. This can be seen in figure 4.5 in which the spin expectation value of the analytical solution is plotted together with

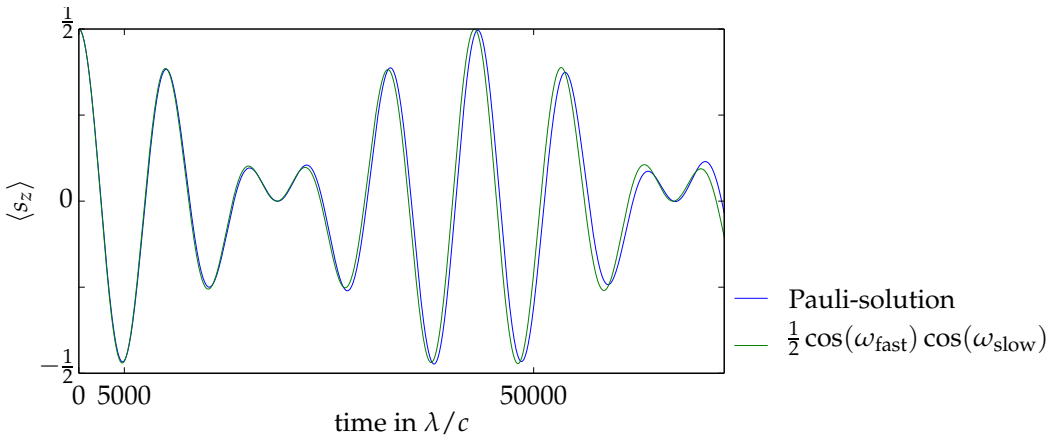

Figure 4.5: Spin expectation value of the analytical solution of the linear system (4.18) truncated after the third mode with small terms neglected. The green line represents the numerically found spin law (4.10). The light is circularly polarized and its parameters are $\hat{E} = 400\,\text{a.u.}$ and $\lambda = 3\,\text{a.u.}$. These are the same parameters as in figure 4.1.

the numerically found spin law (4.8). The solution of this system is a very long and complicated expression. It should be possible to retrieve an analytical expression for ω_{slow} by means of approximations and simplifications of this solution. Initial attempts were fruitless in this regard. Neverthelesss, it is possible to validate the numerically found laws (4.8) (4.9) (4.10) for the spin precession by means of plots (see figure 4.6). These laws are consistent with the analytical solution. But this means conversely that this solution is inconsistent with the numerical findings for small wavelengths because it lacks the exponential law found numerically in this regime (see figure 4.4(b)).

There are several possible reasons for this discrepancy. Because the resonance condition (2.18) has to be fulfilled, the wavelength of the light is inversely proportional to the electron momentum. Therefore the electron momentum increases for small wavelengths. As a result, the neglection of the last three terms in the Fouldy-Wouthuysen transformed Dirac equation (4.11) could be too harsh in this regime. Furthermore, it is possible that the truncation of the linear system (4.18) is not valid in this regime because higher modes might become important for smaller wavelengths. Another possibility is the neglection of the χ term (4.22) in (4.18) as this term is inversely proportional to the wavelength of the light. Unfortunately, these questions remain unanswered in this thesis and this chapter ends here.

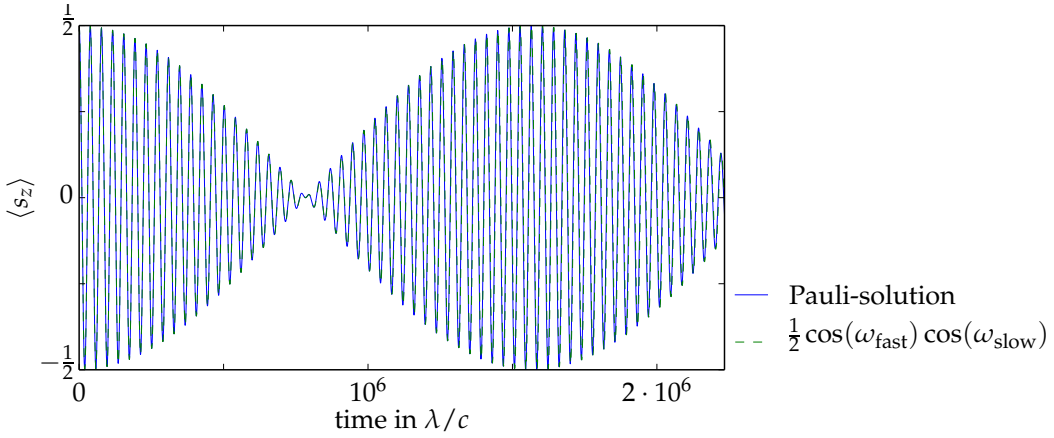

(a) $\eta = \pi/2$

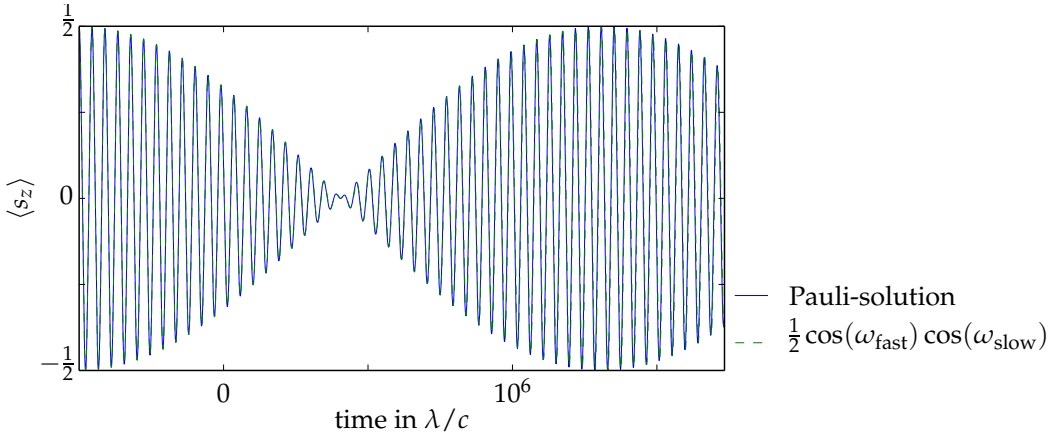

(b) $\eta = \pi/3$

Figure 4.6: These figures show the same functions as figure 4.5 but with a different parametrization. The light parameters are $\hat{E} = 300$ a.u. and $\lambda = 2$ a.u. and two different ellipticities are used.

5 Conclusion

The aim of this work was to investigate the two-photon Kapitza-Dirac effect for which the light waves are elliptically polarized. In contrast to the standard configuration, that is linear polarization, additional effects arise. Two fundamentally different setups are covered in the chapters 3 and 4. One setup covers the case in which the two light waves that compose the standing light wave have equal helicity. The electromagnetic fields rotate here in opposite directions. Therefore this case is often reffered to as counterrotating case in this thesis. In the other setup the fields corotate and have opposite helicity.

The numerical results of the counterrotating case in which the light waves have equal helicity can be summarized as follows. The scattering process becomes suppressed for elliptical polarization. The Rabi cycles between the two quantum states corresponding to positive and negative momenta become longer for elliptical polarizaton. This means that longer interaction times are necessary for the electron to be reflected with a certain probability. For circular polarization the necessary time is infinite and thus the effect is completely suppressed. Each light wave by itself would lead to a time dependent spin expectation value for the electron. But the effects of both light waves together cancel each other in this regard. The spin expectation value of the electron is therefore conserved. A Schrödinger equation with a time independent ponderomotive potential describes this system well as shown in section 3.2. This case of equal helicity is thus very akin to the standard configuration.

In the corotating case in which the light waves have opposite helicity the numerical findings are the following. The frequency of the Rabi flopping between quantum states of positive and negative momenta is independent of ellipticity.
For sufficiently long interaction times the spin expectation value oscillates according to $\langle s_z \rangle = \frac{1}{2}\cos(\omega_{\text{fast}} t)\cos(\omega_{\text{slow}} t)$. This oscillation governed by two frequencies denoted ω_{fast} and ω_{slow}. The fast spin precession without the envelope $\cos(\omega_{\text{slow}} t)$ coincides with a spin precession Bauke and others [24] found for an electron at rest in the same setup for circular polarization. The dynamics of this system can to be replicated to some extent by means of a relativistic Pauli equation with a time independent Hamiltonian, which is done in section 4.2.

Bibliography

[1] P. L. Kapitza and P. A. M. Dirac. The reflection of electrons from standing light waves. *Mathematical Proceedings of the Cambridge Philosophical Society*, 29:297–300, 5 1933.

[2] Phillip L. Gould, George A. Ruff, and David E. Pritchard. Diffraction of atoms by light: The near-resonant Kapitza-Dirac effect. *Phys. Rev. Lett.*, 56:827–830, Feb 1986.

[3] Peter J. Martin, Bruce G. Oldaker, Andrew H. Miklich, and David E. Pritchard. Bragg scattering of atoms from a standing light wave. *Phys. Rev. Lett.*, 60:515–518, Feb 1988.

[4] P. H. Bucksbaum, D. W. Schumacher, and M. Bashkansky. High-intensity Kapitza-Dirac effect. *Phys. Rev. Lett.*, 61:1182–1185, Sep 1988.

[5] Daniel L. Freimund, Kayvan Aflatooni, and Herman Batelaan. Observation of the Kapitza-Dirac effect. *Nature*, 413(6852):142–143, Sep 2001.

[6] Louis de Broglie. *Recherches sur la théorie de quanta*. PhD thesis, Paris, 1924.

[7] H. Batelaan. The Kapitza-Dirac effect. *Contemporary Physics*, 41(6):369–381, 2000.

[8] Bernd Thaller. *Advanced Visual Quantum Mechanics*. Springer, 2005.

[9] Eckhard Rebhan. *Theoretische Physik: Relativistische Quantenmechanik, Quantenfeldtheorie und Elementarteilchentheorie*. Springer, 2010.

[10] Jürg Fröhlich and Urban M. Studer. Gauge invariance and current algebra in nonrelativistic many-body theory. *Rev. Mod. Phys.*, 65:733–802, Jul 1993.

[11] Richard A. Beth. Mechanical detection and measurement of the angular momentum of light. *Phys. Rev.*, 50:115–125, Jul 1936.

[12] J. Humblet. Sur le moment d'impulsion d'une onde électromagnétique. *Physica*, 10(7):585 – 603, 1943.

[13] Stephen M. Barnett. On the six components of optical angular momentum. *Journal of Optics*, 13(6):064010, 2011.

[14] Sven Ahrens. *Investigation of the Kapitza-Dirac effect in the relativistic regime*. PhD thesis, Ruprecht-Karls Universität Heidelberg, 2012.

[15] Heiko Bauke, Sven Ahrens, Christoph H. Keitel, and Rainer Grobe. Electron-spin dynamics induced by photon spins. *New Journal of Physics*, 16(10):103028, 2014.

[16] Heiko Bauke and Christoph H. Keitel. Accelerating the Fourier split operator method via graphics processing units. *Computer Physics Communications*, 182:2454–2463, Dec 2011.

[17] Franz Schwabl. *Quantenmechanik für Fortgeschrittene (QM II)*. Springer, 2008.

[18] Thiab R Taha and Mark I Ablowitz. Analytical and numerical aspects of certain nonlinear evolution equations. ii. numerical, nonlinear schrödinger equation. *Journal of Computational Physics*, 55(2):203 – 230, 1984.

[19] Wilhelm Magnus. On the exponential solution of differential equations for a linear operator. *Communications on Pure and Applied Mathematics*, 7(4):649–673, 1954.

[20] Per Christian Moan and Jitse Niesen. Convergence of the Magnus series. *Foundations of Computational Mathematics*, 8(3):291–301, 2008.

[21] S. Blanes, F. Casas, J.A. Oteo, and J. Ros. The Magnus expansion and some of its applications. *Physics Reports*, 470(5–6):151 – 238, 2009.

[22] S Blanes, F Casas, J A Oteo, and J Ros. A pedagogical approach to the Magnus expansion. *European Journal of Physics*, 31(4):907, 2010.

[23] E. D. Landau and E. M. Lifshitz. *Mechanics*, volume 2. Pergamon Press, 1969.

[24] Heiko Bauke, Sven Ahrens, and Rainer Grobe. Electron-spin dynamics in elliptically polarized light waves. *Phys. Rev. A*, 90:052101, Nov 2014.

Erklärung

Ich versichere, dass ich diese Arbeit selbstständig verfasst und keine anderen als die angegebenen Quellen und Hilfsmittel benutzt habe.

Heidelberg, den